PHILOSOPHICAL TRANSACTIONS OF THE ROYAL SOCIETY A MATHEMATICAL, PHYSICAL & ENGINEERING SCIENCES

# The interaction of solutes with their environments

G. R. Fleming, S. A. Passino and Y. Nagasawa

*Phil. Trans. R. Soc. Lond. A* 1998 **356**, doi: 10.1098/rsta.1998.0172, published 15 February 1998

The Royal Society

# The interaction of solutes with their environments

By G. R. Fleming[1], S. A. Passino[2] and Y. Nagasawa[2]

[1]*Department of Chemistry, University of California, Berkeley, CA 60637, USA*
[2]*Department of Chemistry, The University of Chicago, Chicago, IL 94720, USA*

The origins of electronic spectral broadening in solutions, glasses and proteins are discussed via three pulse stimulated echo peak-shift measurements. Spectral densities for dye molecules in polar solutions are presented and discussed in terms of molecular models for the dynamics. The breakdown of the harmonic bath picture at low frequencies is presented. Finally, echo measurements on light harvesting complexes of purple bacteria are presented and it is shown that the energy transfer timescale can be obtained from peak-shift measurements.

**Keywords: femtosecond spectroscopy; solvation dynamics; nonlinear spectroscopy; spectral broadening; photon echoes**

## 1. Introduction

The optical absorption spectra of molecules dissolved in liquids, glasses and proteins are deceptively bland. Figure 1 shows absorption spectra for the dye IR144 in dilute methanol solution and in dilute solution in the polymer glass PMMA, both at room temperature. The spectra are extremely similar in shape, even though one expects very different timescales for the solvent motion in the two cases. In the glass we expect static inhomogeneity—i.e. site energy differences that persist for times enormously longer than the experimental time window, whereas the fluid solution is expected to be 'homogeneous' on timescales longer than a few tens of picoseconds. Can we disentangle the various sources of spectral broadening and obtain a description of the solute–solvent interaction that can be transferred to other situations such as reactions in the same environment? In this paper we will focus on one particular experimental technique—the three pulse stimulated echo peak-shift measurement (Nagasawa *et al.* 1997; de Boeij *et al.* 1995, 1996; Joo *et al.* 1996*a*,*b*; Passino *et al.* 1996) and show how it can be used to obtain both static and dynamical contributions to the line broadening. We characterize the dynamical contributions by means of a spectral density, $\rho(\omega)$ (Cho *et al.* 1996; Fleming & Cho 1996). The spectral density characterizes the range and distribution of timescales weighted by how strongly they influence the quantity in question. In other words, if we represent the solvent bath by a set of harmonic oscillators, the spectral density is simply a coupling constant weighted density of states, i.e.

$$\rho(\omega) \equiv \frac{1}{2\hbar} \sum_{\infty} \frac{c_\alpha^2}{m_\alpha \omega_\alpha^3} \delta(\omega - \omega_\alpha). \tag{1.1}$$

Once $\rho(\omega)$ is obtained, the challenge is to interpret it in molecular terms and to use it for predictive purposes. To take a specific example, quantitative application

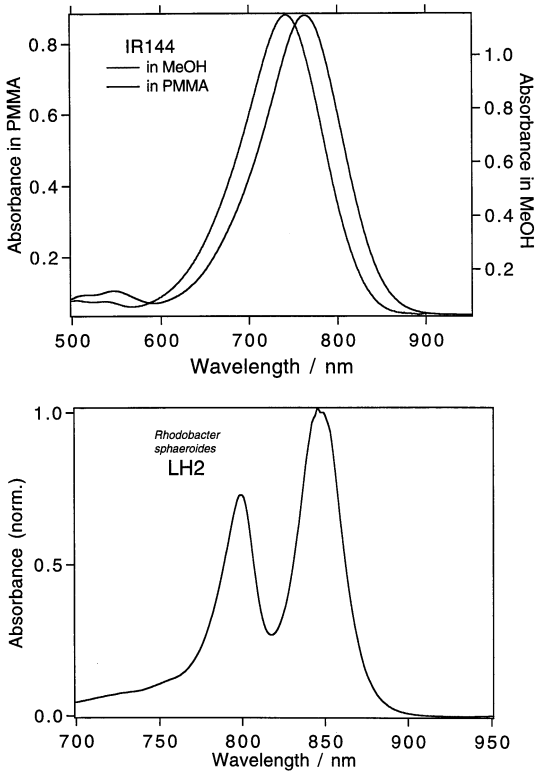


Figure 1. Absorption spectra of various solutes. (Upper panel) IR144 in dilute solution in a fluid solvent (methanol) and a polymer glass (PMMA) at 300 K. (Lower panel) Light harvesting complex 2 from the purple bacterium *Rhodobacter sphaeroides*. The two bands at 800 and 850 nm are related to the two rings of bacteriochlorophyll molecules in this structure.

of the spectral density to predict the influence of temperature on electron transfer reactions requires us to confront the issue of whether the solvent motion can really be described as harmonic or not (Cho & Fleming 1998). We note in passing that the assumption of parabolic free energy curves is a far less restrictive assumption than that of taking the individual solvent motions to be governed by a coupling potential operator which is quadratic in its coordinates (Marcus & Sutin 1985).

Figure 1 also contains the absorption spectrum of a far more complex system, the light harvesting-2 complex (LH2) of purple bacteria. LH2 consists of a ring composed of nine $\alpha$, $\beta$ pairs of membrane-spanning helices, each $\alpha$, $\beta$ pair containing three bacteriochlorophyll (BChl) molecules (McDermott *et al.* 1995). One BChl molecule (B800) is monomeric in the complex, whereas the B850 pair interact strongly with each other and with their neighbours in the next $\alpha\beta$ subunits. LH2 transfers energy to LH1 which is based in a similar structural principle (McDermott *et al.* 1995). In LH1, 16 $\alpha\beta$ helices hold 32 BChls (B875). The reaction centre is believed to sit in the centre of the LH1 ring, and very rapid energy migration occurs between the 32 BChl molecules. Energy transfer to the special pair ($P$) of the reaction is comparatively slow at 35 ps (McDermott *et al.* 1995; Karrasch *et al.* 1995) and constitutes the rate limiting step of the light harvesting process.

In such a complex system as LH2, even the simplest analyses of linear spectra are compromised. For example, in the dilute systems mentioned above the total

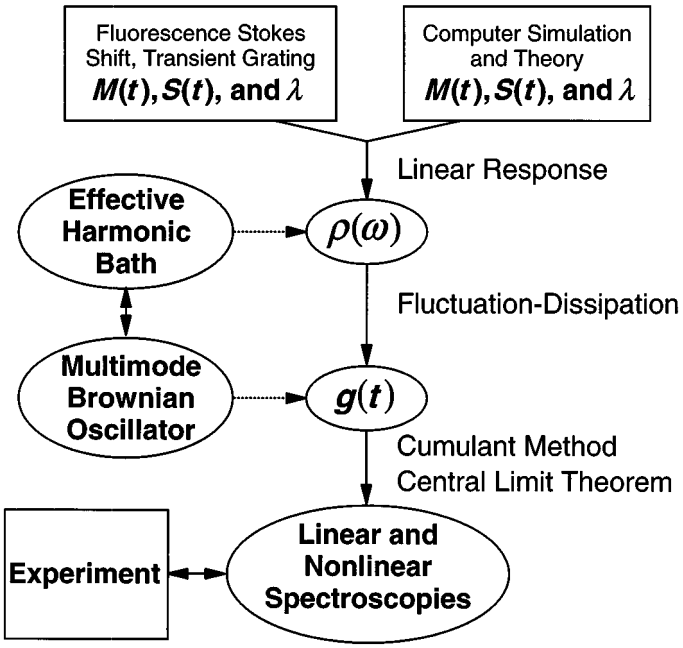


Figure 2. Calculation procedure for linear and nonlinear spectroscopic signals based on the harmonic spectral density model.

coupling of the electronic transition to nuclear degrees of freedom (the reorganization energy, $\lambda$) can be obtained as half the Stokes shift between the absorption and emission spectra. In a system with energy transfer and disorder, this is no longer possible, since now emission comes from a different molecule than the one that was initially excited.

Ultrafast nonlinear spectroscopy provides a means of dealing with the obfuscation created by the various line broadening mechanisms present in figure 1. There are two broad classes of approaches. The first simply exploits the fact that dynamical events such as bond breaking can be initiated on times shorter than that characterizing the nuclear motion. Thus, the whole ensemble is set in motion at once, and as long as the wavepacket so created remains intact, the chemical events can be followed directly in real time, even for systems with completely structureless spectra (Jonas *et al.* 1993, 1995*a*; Gruebele & Zewail 1993; Scherer *et al.* 1993; Pollard *et al.* 1990). The alternative approach, and the one we will consider in this paper, is to exploit various forms of echo spectroscopy to study and manipulate the mechanisms of line broadening. The key concept in this approach and the link to understanding and predicting dynamics is the spectral density, $\rho(\omega)$. Figure 2 shows the relationship of the spectral density to various key quantities. Before taking up some of the issues posed by figure 2, we pause to consider the spectral density and its relationship to observables in a little more detail.

Consider a chromophore, $i$, in dilute solution. We can consider the optical transition energy, $\Delta E^i$, between ground and excited states to be composed of three contributions: an average value for the whole ensemble, $\langle \Delta E \rangle$; a dynamical part arising from fluctuations in the environment and the molecule itself, $\delta_{\mathrm{SB}}(t)$; and an offset from the mean transition energy, $E_i$. The width of the distribution of $E_i$ values, $\Delta_{\mathrm{in}}$,

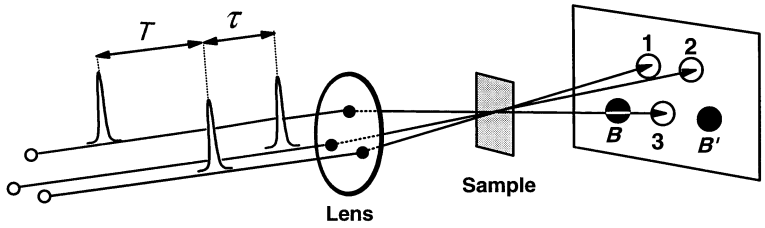


Figure 3. Experimental arrangement for stimulated three pulse echo signals. $B$ and $B'$ correspond to the three pulse stimulated echoes at $\boldsymbol{k}_1-\boldsymbol{k}_2+\boldsymbol{k}_3$ and $-\boldsymbol{k}+\boldsymbol{k}_2+\boldsymbol{k}_3$, respectively. The population period, $T$, and the initial (coherence) period, $\tau$, are indicated.

corresponds to the width of the inhomogeneous distribution:

$$\Delta E^i(t) = \langle \Delta E \rangle + \delta V^i_{\mathrm{SB}}(t) + E_i. \tag{1.2}$$

To proceed, we assume that the fluctuations are similar for all members of the ensemble. Then the time dependence of the Stokes shift, $S(t)$, is given by

$$S(t) = \frac{\langle \delta V_{\mathrm{SB}}(t) \delta V_{\mathrm{SB}}(o) \rangle}{\langle \delta V^2_{\mathrm{SB}} \rangle}, \tag{1.3}$$

$$S(t) = \frac{\hbar}{\lambda} \int_0^\infty \mathrm{d}\omega\, \omega \rho(\omega) \cos(\omega t) \tag{1.4}$$

and the reorganization energy, $\lambda$, is given by

$$\lambda = \hbar \int_0^\infty \mathrm{d}\omega\, \omega \rho(\omega). \tag{1.5}$$

Similarly, all linear and nonlinear signals can be obtained from the lineshape function, $g(t)$, that can also be written in terms of $\rho(\omega)$ and the temperature (Cho *et al.* 1996; Fleming & Cho 1996; Mukamel 1995).

From the experimental perspective, then, what we require is a technique that can determine both the timescales (or spectrum) and amplitude of the fluctuations, i.e. the spectral density, and the inhomogeneous distribution width, $\Delta_{\mathrm{in}}$. Fluorescence Stokes shift measurements can give $\rho(\omega)$ via inversion of (1.4), but are insensitive to $E_i$ since only population dynamics are measured (Cho *et al.* 1996; Fleming & Cho 1996). Echo spectroscopies on the other hand can give both $\rho(\omega)$ and $\Delta_{\mathrm{in}}$ (Cho *et al.* 1996; Fleming & Cho 1996).

## 2. The three-pulse stimulated echo peak-shift (3PEPS) method

Various types of echo spectroscopy have been discussed in detail recently (Nagasawa *et al.* 1997; de Boeij *et al.* 1995, 1996; Joo *et al.* 1996*a*,*b*; Passino *et al.* 1996) and only a brief outline will be given here. Figure 3 shows the pulse sequence and definition of the peak shift $\tau^*(T)$ for 3PEPS. The key features of the technique are as follows. The second time period $T$ corresponds to propagation in a diagonal density matrix (i.e. a 'population' state) and thus provides a long time period for the system to explore its environment compared to techniques in which only superpositions (coherences) are exploited. Secondly, by measuring the position of the two time-reversed images of the integrated stimulated echo signal, the shift of the peak of the integrated echo from the time origin ($\tau = 0$) can be determined with very high precision ($\pm 300$ as). The quantity of interest $\tau^*(T)$ versus the population period $T$

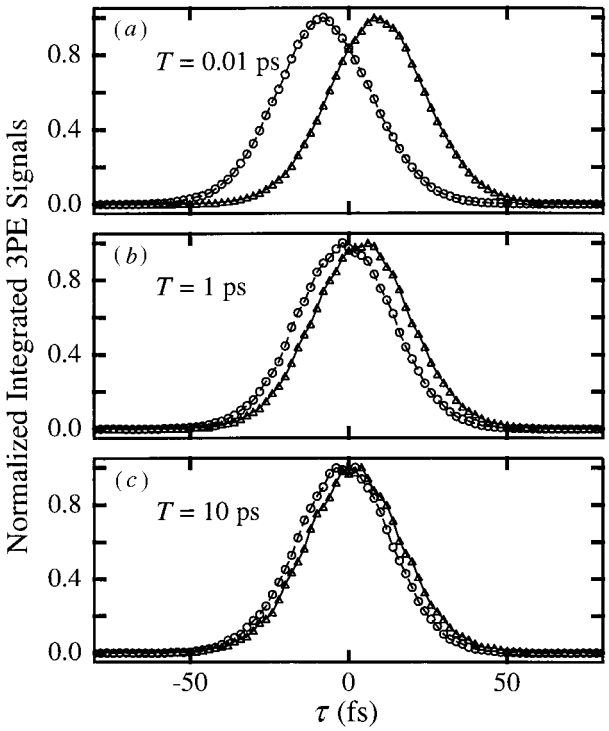


Figure 4. Stimulated echo signals observed at $B$ and $B'$ of figure 3 for IR144 in methanol. ($a$), ($b$) and ($c$) were recorded for population periods of $T = 0.01$, $T = 1$ and $T = 10$ ps, respectively.

can then be obtained from data such as those in figure 4. As the population period is increased, the two signals approach each other. If the two peaks overlap completely ($\tau^* = 0$) then the system has explored all the environments in the ensemble. If, on the other hand, there are environments that are inaccessible on the experimental timescale, the peak shift will never reach zero, but instead decay to a finite long time value, $\tau^*(\infty)$. This distinction is immediately apparent when comparing the data for dilute solutions of the dye IR144 (Maeda 1984) in ethanol and in the polymer glass, PMMA, shown in figure 5. The peak shift in the fluid solution decays to zero on the 100 ps timescale, while the glass data show a constant $\tau^*(\infty)$ value after about 200 fs (Nagasawa *et al.* 1996, 1997; Cho *et al.* 1996). An analysis of the temperature dependence of the glass data of figure 5 is given in the manuscript by Nagasawa (1997). The oscillations evident in all the curves result from vibrational wavepackets. A striking feature of the two room temperature curves is the great similarity of the signals up to *ca.* 180 fs. In part, this results from the contributions of intramolecular vibrational modes to the short time dynamics, but it also shows that the short time solvent response is very similar in the liquid and the glass. In other words, the liquid behaves like a glass for times short compared to the diffusive timescale. A final point to be made is that in the fluid system, for $T$ values greater than the correlation time (Mukamel 1995) of $S(t)$ (equation (1.3)), the time dependence of $\tau^*(T)$ corresponds exactly to that of $S(t)$ (Cho *et al.* 1996; Fleming & Cho 1996). To extract the shorter time behaviour of $S(t)$ and hence the higher-frequency components of $\rho(\omega)$ from the peak shift data requires numerical modeling in which the finite duration of the light fields is included explicitly (de Boeij *et al.* 1996; Joo *et al.* 1996*a*). We now turn to a discussion of spectral densities that have been extracted from such measurements.

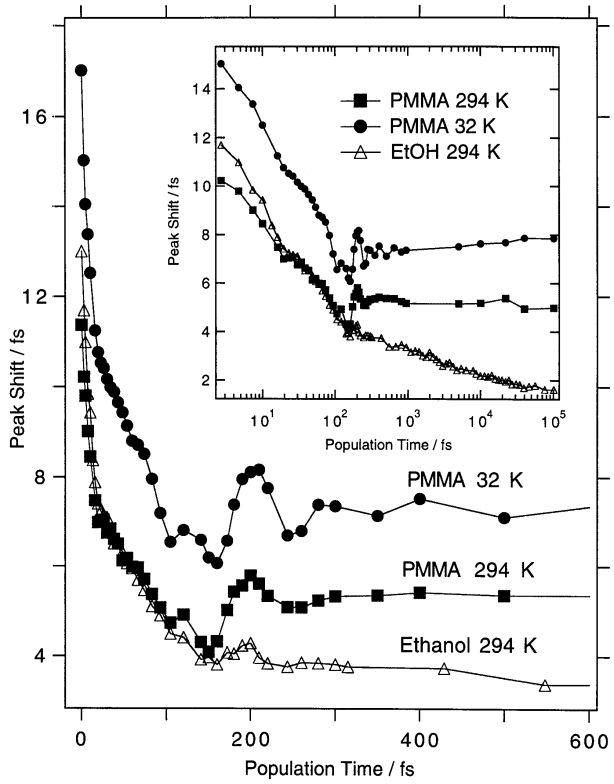


Figure 5. Peak shift ($\tau^*$) as a function of population period ($T$) for IR144 in ethanol (triangles) at 294 K and in PMMA at 294 K (squares) and 32 K (solid circles). The inset shows data to 100 ps on a logarithmic time scale.

### (*a*) *Experimental spectral densities*

Figure 6 shows the spectral density (weighted by $\omega^2$) obtained for methanol solutions of the dye IR144 (Passino *et al.* 1996). The spectral density consists of a number of clearly identifiable and distinct features. The lowest frequency peak in the spectrum results from the diffusive contribution to the solvation dynamics. In methanol, this contribution is clearly resolved from the broad feature peaking at *ca.* 85 $\mathrm{cm}^{-1}$ which corresponds to the ultrafast (80 fs in $\tau^*$) 'librational' component of the solvent response. The shoulders on the high frequency and side of the librational peak and the distinct peaks at higher frequency all correspond to intramolecular vibrational modes of IR144. They correspond well with features in the Raman spectrum of IR144 in acetonitrile (Vitale & Gustafson, unpublished results). The limited bandwidth of the laser pulses used in this experiment means that high-frequency molecular vibrations are not impulsively excited. In addition, groups of medium-frequency (*ca.* 400–700 $\mathrm{cm}^{-1}$) modes are poorly resolved (Jonas *et al.* 1995*a*,*b*). In our fitting procedure, this leads to the highest-frequency mode having an unrealistically large width (i.e. very short damping time) to account for these effects. Such a lack of time resolution influences the quality of our fit of the peak-shift data for the first 10–20 fs but has little influence for times longer than this.

The rapid progress that has been made in describing polar solvation from several different perspectives gives us the opportunity to examine the molecular origins of spectral densities shown in figure 6. For example, the instantaneous normal mode

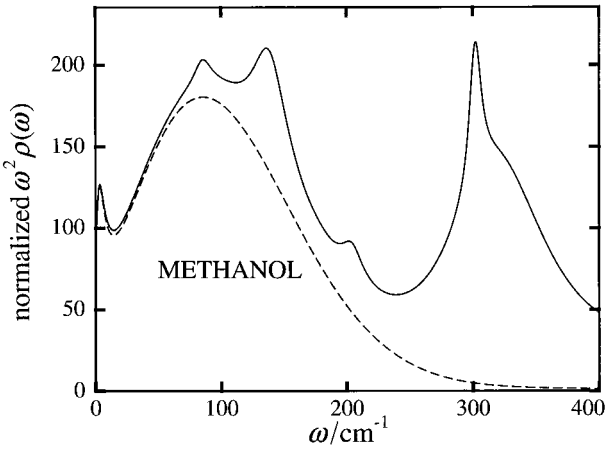


Figure 6. Harmonic ('basis set') spectral density $\rho(\omega)$ obtained from fits to 3PEPS data for IR144 in methanol.

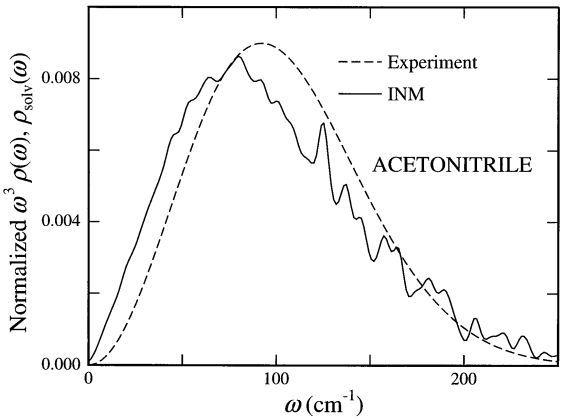


Figure 7. Comparison of the librational portion of the spectral density obtained for acetonitrile (300 K) with IR144 as a probe and the INM spectral density ($\rho_{\mathrm{solv}}$) calculated by Ladanyi & Stratt (1995). Because the INM calculation uses only harmonic modes, the diffusive peak on the low-frequency side of the experimental data is not captured.

(INM) approach developed by Stratt and co-workers, and Keyes and co-workers (Ladanyi & Stratt 1995, 1996; Stratt 1995; Cho *et al.* 1994; Keyes 1994; Stratt & Cho 1994) allows us to ask what types of molecular motion contribute to the librational peak which is prominent in all systems studied so far. (Since, at present, the INM approach to solvation dynamics (Ladanyi & Stratt 1995, 1996; Stratt 1995; Cho *et al.* 1994; Keyes 1994; Stratt & Cho 1994) is restricted to harmonic modes, and thus, the system is stuck in a given set of minima and diffusion cannot occur. Thus the INM solvation spectral density does not contain the diffusive peak.) In figure 7 we compare the librational peak obtained for acetonitrile (this time normalized by $\omega^3$) with the INM solvation spectrum ($\rho_{\mathrm{solv}}$) of acetonitrile calculated by Ladanyi & Stratt (1995). The similarity of the two spectra is remarkable, the more so since the calculated spectrum predates the experimental result! The similarity of experimental and INM solvation spectra allow us to use the decomposition of the INM solvation spectrum made by Ladanyi & Stratt (1995). These authors found that the solvation spectral density rather closely followed the rotational contribution to the

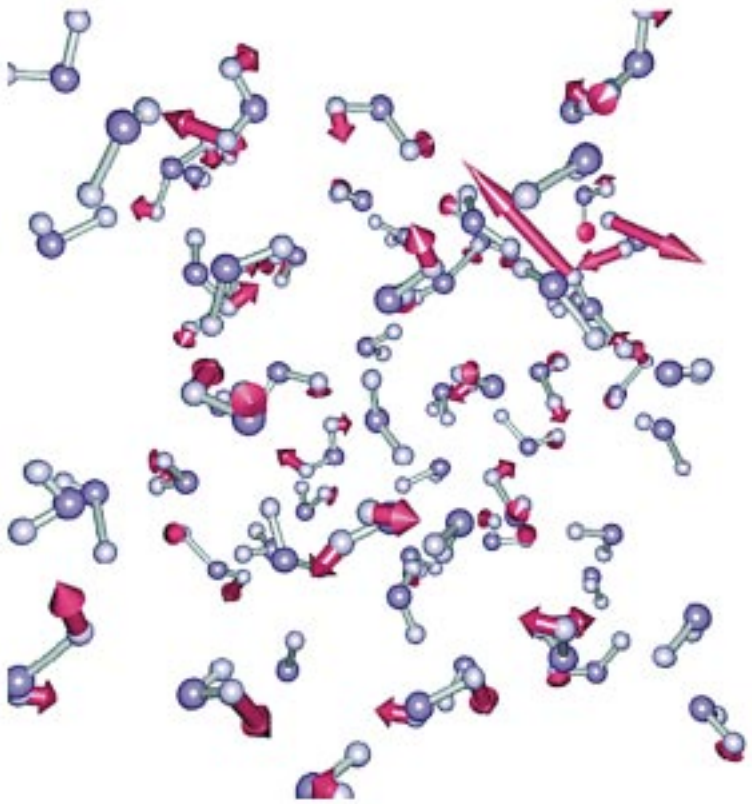

Figure 8. An INM calculated for water by Saito & Ohmine (Cho *et al.* 1994). The mode shown has a frequency of 752 $cm^{-1}$ and is rotational in nature. Displacement vectors are shown on the water hydrogen atoms, and the rotational motion of many of the molecules contributing to this mode is clear. In general, rotational motions such as this are dominating the solvation dynamics.

total spectral density and that translational motions contributed little to the solvation dynamics, at least in the sub 100 fs time regime (see figure 4 of Ladanyi & Stratt 1995). The solvation spectral density does peak at slightly higher frequency than the rotational contribution to the normal mode spectrum suggesting that higher-frequency rotational-type modes are somewhat more effective at relaxing the solvation energy. A feeling for what type of motion is involved in rotational-type INM can be obtained from figure 8 which shows the INM displacement vectors for a 752 $cm^{-1}$ rotational INM of water calculated by Saito & Ohmine (Cho *et al.* 1994). The arrows on the water hydrogen atoms indicate the magnitude of the individual displacement vectors, and the rotational nature of the motion is clearly apparent. We emphasize that a single mode is shown here—all the vectors belong to the same mode; in water we have found that typically 50–80 water molecules make some contribution to each individual INM (Cho *et al.* 1994), though the number making large contributions is significantly less, as is evident from figure 8.

If a harmonic model provides a good description of the ultrafast component of solvation, we should expect this component to be very insensitive to changes in temperature. In models in which the bath Hamiltonian is written as a set of harmonic oscillators linearly coupled to the optical transition, the only temperature dependence comes from the Bose occupation numbers of the harmonic modes; the spectral

density itself, and hence the reorganization energy, are strictly temperature independent. We have investigated this point in two systems: a polymer glass (PMMA) between 300 and 30 K (Nagasawa *et al.* 1996, 1997; Cho *et al.* 1996), and ethylene glycol solution between 300 and 400 K (Passino *et al.* 1997). In both cases, the probe molecule was IR144. In the glass sample, as figure 5 shows, the diffusive contribution to the dynamics is completely lacking and is replaced by static offset representing the inhomogeneous broadening. The fast component ascribed to librational motions in the glass is remarkably temperature independent. The room temperature spectral density, in combination with the fluctuation dissipation theorem, is able to account for the lack of temperature dependence very well (Nagasawa *et al.* 1997). The only feature of the glass data not well described over the whole range is the long-time ($\tau^*(T \rightarrow \infty)$ value of the peak shift. We will not pursue the origin of this discrepancy further here.

The liquid phase, at least at atmospheric pressure, gives less scope for changes of temperature. However, high-quality data at 400 K were acquired for IR144 in ethylene glycol (Passino *et al.* 1997) for comparison with room temperature data. Again, the librational ultrafast dynamics, while extremely insensitive to the temperature and the spectral density between 10 and 250 $\mathrm{cm}^{-1}$ (in $\omega^2\rho(\omega)$), is very similar at 297 and 397 K. For the lower-frequency range of the spectral density (0–10 $\mathrm{cm}^{-1}$ in $\omega^2\rho(\omega)$) the situation is strikingly different (figure 9). This region corresponds to the diffusive portion of the solvation and *a priori* is very unlikely to be harmonic in character. At this point we should remark on a distinction in our various uses of the word harmonic. If one regards the solvent as a set of harmonic oscillators, it is possible to view this model in at least two ways. In the INM approach the frequencies correspond to specific (instantaneous) modes and can be directly related to the motions of the molecules. A more general approach is to regard the harmonic oscillators as a 'basis set' which simply characterizes the range of timescales and coupling strengths of the bath. This latter approach is very general and can always be parameterized to fit an individual experimental result. However, when experiments are performed at various temperatures, for example, the ability to make prediction from data at a single temperature depends strongly on whether the motions are indeed harmonic. Clearly the harmonic model holds quite well for ethylene glycol for frequencies above 10–20 $\mathrm{cm}^{-1}$ (in $\omega^2\rho(\omega)$), but fails badly below this range.

This failure of the harmonic model in the low-frequency region has led us to examine a number of intrinsically anharmonic models of polar solvation, which at least in principle can describe the whole range of timescales from ultrafast (less than or equal to 100 fs) to tens or hundreds of picoseconds.

### (*b*) *Molecular descriptions of polar solvation dynamics*

Over the past ten years, great progress has been made in developing molecular-level descriptions of the relaxation of polar liquids around charged or dipolar solutes. The initial breakthrough came with the formulation of the dynamical form of the mean spherical approximation (DMSA) by Wolynes (1987), and its elaboration by other groups (Rips *et al.* 1988). Maroncelli and co-workers have explored this model and the simple continuum model (Böttcher & Bordewijk 1978; Frölich 1958) in the context of their extensive fluorescence Stokes shift data for coumarin-153 (Maeda 1984; Horng *et al.* 1995). These workers find that the DMSA approach for ions provides a reasonable description for most solvents. Acetonitrile appears to be an exception in this regard; for this solvent, the DMSA-dipole approach gave a result

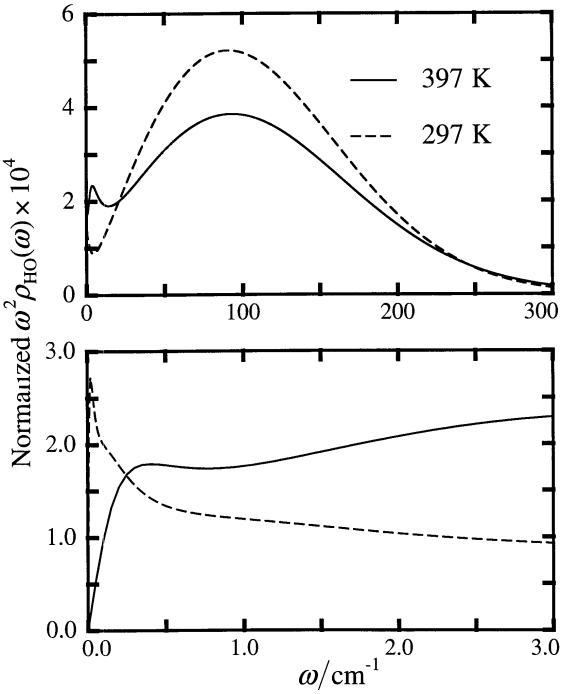


Figure 9. Harmonic ('basis set') spectral densities for ethylene glycol obtained using IR144 as a probe at 297 K (solid line) and 397 K (dashed line). The librational frequency region is quite similar at the two temperatures, but the lower-frequency (diffusive) region is strikingly different at the two temperatures.

closer to experiment, although in general DMSA-dipole responses are significantly slower than the experimentally observed timescales (Horng *et al.* 1995). Perhaps the most sophisticated approach to date is the XRISM (extended reference interaction site model) work of Raineri & Friedman (Raineri *et al.* 1994, 1997; Friedman *et al.* 1994, 1995), which extends the RISM approach of Chandler & Anderson (1972) to the dynamical case.

The key point about all the models mentioned above is that they do not rely on any assumption of harmonicity of the molecular motions. The simple continuum (SC) and DMSA models generate a susceptibility via the frequency- and wavevector-dependent complex dielectric function

$$\varepsilon(\boldsymbol{k},\omega) = \varepsilon'(\boldsymbol{k},\omega) - \mathrm{i}\varepsilon''(\boldsymbol{k},\omega). \tag{2.1}$$

In the case of the SC model, since molecular size is neglected, only the zero wavevector component, i.e. $\varepsilon(\boldsymbol{k}=0,\omega)$, enters. The DMSA treats the liquid as a dipolar hard sphere fluid and the ratio of solute–solvent sizes can be incorporated into the model. Both the SC and DMSA generate the Stokes shift function, $S(t)$ (equation (1.3)), via a susceptibility $\chi(\varepsilon(\boldsymbol{k},\omega))$ which is a function of the complex dielectric response (Wolynes 1987; Rips *et al.* 1988)

$$L^{-1}[S(t)] = \int_0^\infty \mathrm{d}^3k\, \frac{[\chi[\varepsilon(\boldsymbol{k},0)] - \chi[\varepsilon(\boldsymbol{k},\omega)]]}{\mathrm{i}\omega[\chi[\varepsilon(\boldsymbol{k},0)] - \chi[\varepsilon(\boldsymbol{k},\infty)]]}, \tag{2.2}$$

where $L^{-1}$ denotes the inverse Laplace transform (we defined the Laplace inverse as $L^{-1}[S(t)] \equiv \int_0^\infty \mathrm{d}t\, \mathrm{e}^{-pt} S(t)$ with $p = \mathrm{i}\omega$). From equation (1.4) this leads to a relation

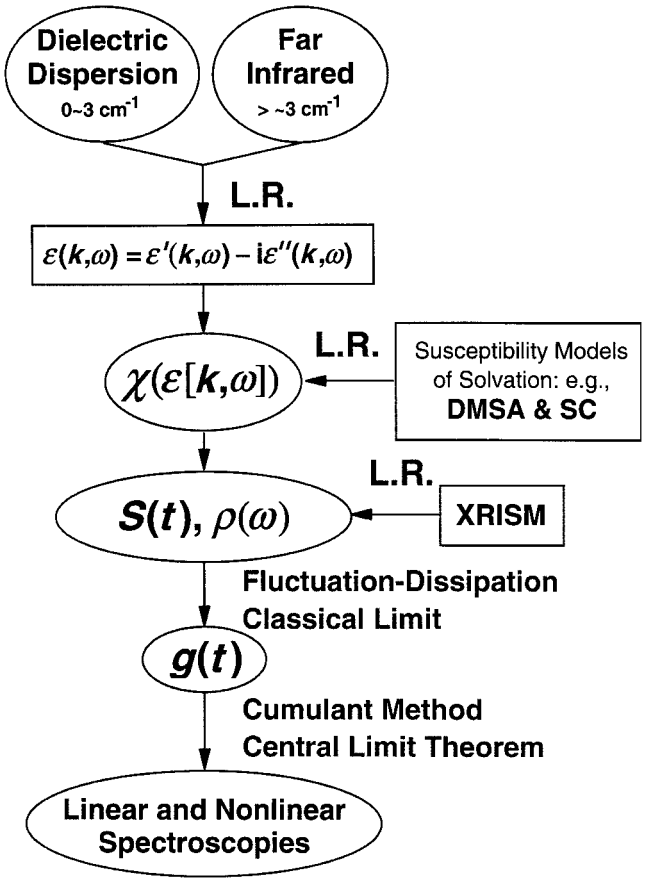


Figure 10. Calculation procedure for modeling linear and nonlinear spectroscopies using various models of solvation. SC = simple continuum; DMSA = dynamic mean spherical approximation; XRISM = extended reference site interaction model. LR indicates linear response.

between the DMSA or SC spectral density $\rho_{\mathrm{SM}}(\omega)$ (Passino *et al.* 1997), and the susceptibility

$$\frac{\hbar\pi\omega^2\rho_{\mathrm{SM}}(\omega)}{2\lambda} = \mathrm{Im}\left\{\int_0^\infty \mathrm{d}^3k\,\frac{[\chi[\varepsilon(\boldsymbol{k},0)]-\chi[\varepsilon(\boldsymbol{k},\omega)]]}{[\chi[\varepsilon(\boldsymbol{k},\infty)]-\chi[\varepsilon(\boldsymbol{k},0)]]}\right\}. \tag{2.3}$$

Here, the subscript SM denotes the spectral density for these susceptibility models. Thus, if $\varepsilon(\boldsymbol{k},\omega)$ is known or can be calculated, the spectral density can be calculated directly and compared with experimental results (Passino *et al.* 1997). Our procedure for obtaining $S(t)$ from $\varepsilon(\boldsymbol{k}=0,\omega)$ follows that of Maroncelli and co-workers (Horng *et al.* 1995). Alternatively, the peak shift itself, $\tau^*(T)$, can be calculated and compared with the experimental result. The calculation procedure is outlined in figure 10. If only the $\varepsilon(\boldsymbol{k}=0,\omega)$ component is used, as is the case in the calculations described here, the integration over phase space in equations (2.2) and (2.3) is not necessary.

In the case of the more realistic (and complex!) XRISM, we obtained spectral densities, $\rho_{\mathrm{XRISM}}$, from equation (1.4) using $S(t)$ functions for acetonitrile and methanol provided to us by Professors Raineri and Friedman (Raineri *et al.* 1997; Raineri &

Friedman 1998). These calculations are based on 19 interaction sites of coumarin-153 and generate a theoretical $\varepsilon(\boldsymbol{k}, \omega)$ from classical molecular dynamics simulation.

For the SC and DMSA models, the quality of the calculated spectral densities clearly depends strongly on the quality of the input dielectric and far infrared data. For ethylene glycol, this is a serious problem as we were unable to find any far infrared absorption data above *ca.* 3 $\mathrm{cm}^{-1}$. For this solvent, we will restrict our discussion to the diffusive portion of the spectral density ($10^{-2}$–10 $\mathrm{cm}^{-1}$). Figure 11 shows calculated $\rho_{\mathrm{SM}}$ for ethylene glycol at 300 K for four different susceptibility models: the SC for ions and dipoles; and the DMSA for the same pair of solutes. Dielectric data from $6.6 \times 10^{-3}$–2.3 $\mathrm{cm}^{-1}$ were used and the upper-limit value is shown by arrows in the figure (Jordan *et al.* 1978). The DMSA–dipole model gives rather striking agreement with the spectral density obtained directly from fitting the peak shift data with the procedure depicted in figure 2 (circles). We emphasize that there are no adjustable parameters for the DMSA and SC model spectral densities, since the complex relative permittivity in the continuum limit were obtained from experimental dielectric dispersion data (Jordan *et al.* 1978). The same complex relative permittivity were used as input for each model, and the differences in the spectral density arise from the approximations inherent to each model. Both the frequency range and the existence of two distinct peaks in $\rho(\omega)$ are reproduced. The other three calculations are rather similar, though a shoulder at *ca.* 0.15 $\mathrm{cm}^{-1}$ is apparent in the DMSA-ion result while the SC spectra are featureless. The structure in the DMSA spectral densities must, therefore, reflect the molecular structure of the hard sphere liquid and in this appear to be more accurately represented by the ion version of the theory.

At 400 K, the two peaks in $\rho(\omega)$ move to higher frequency and change their relative intensities (figure 11*b*). The dielectric data used for the calculations in figure 11*b* involves a large and uncertain extrapolation of data collected between 283 and 313 K up to 397 K. Thus, the results should be regarded as illustrative rather than quantitative. Although the DMSA-ion spectrum shifts to higher frequency and appears to mimic the increase of amplitude of the higher-frequency component compared to the lower-frequency component, the agreement between calculation and experiment is now quite poor, most likely as a result of the unreliability of our extrapolated dielectric data.

Similar calculations, but including the ultrafast solvation component via far infrared absorption data, have been carried out for acetonitrile and methanol and were discussed elsewhere (Passino *et al.* 1997).

We conclude this section with a discussion of XRISM calculations of the full peak-shift signal for IR144 in methanol. In order to perform this calculation, the contributions from intramolecular vibrational modes must be included (Joo *et al.* 1996*b*). Figure 12 shows the calculated and experimental $\tau^*(T)$ versus $T$ curves. The calculated curve uses the $S(t)$ obtained by Raineri & Friedman based on XRISM and their collective reference dynamical variables approach. The calculation of $S(t)$ is fully theoretical in that only simulation data is used as input (Jordan *et al.* 1978; Bertie *et al.* 1993) and is based on a model of coumarin-153 with 19 interaction sites. We expect (aside from the total reorganization energy) little difference between different large probe molecules. In making contact with the experimental data, the only variable is the solvent reorganization energy which simply scales the solvent and intramolecular vibrational contributions to the peak shift. In other words, the value of the reorganization energy does not change the shape of peak-shift curve aside from this. We found for both methanol and acetonitrile that the XRISM approach gave reorgani-

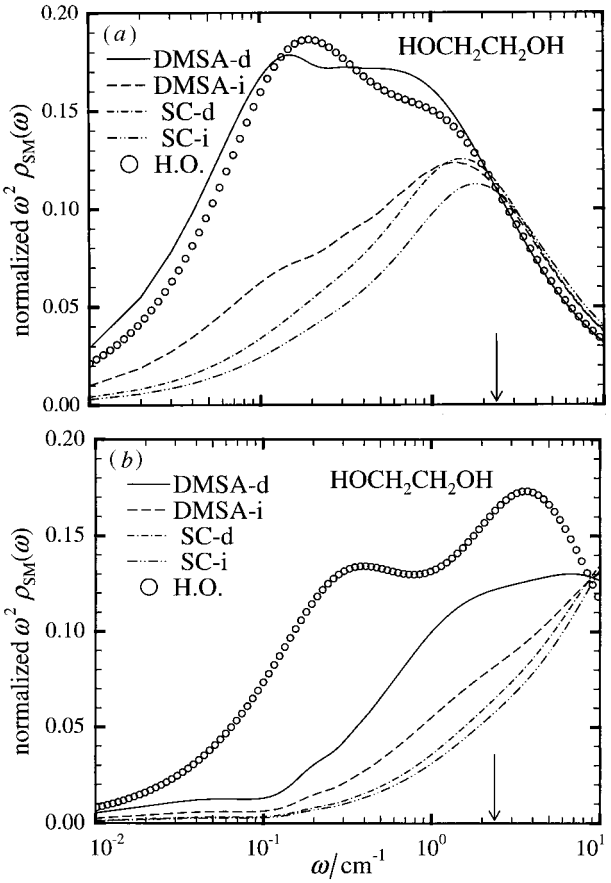


Figure 11. (*a*) Ethylene glycol spectral densities at 297 K calculated according to four susceptibility-based models. The open circles give the experimental spectral density obtained from the harmonic, basis set approach. The arrow indicates the upper limit of the dielectric data used. (*b*) The same at 397 K. The symbols d and i in both figures refer to the dipole or ion forms of the indicated models.

zation energies very similar to those obtained directly from the fluorescence Stokes shift, while the $\lambda$s for the SC and DMSA models were generally significantly too large (Passino *et al.* 1997). Clearly, the agreement between theory and experiment for methanol (and acetonitrile (Passino *et al.* 1997)) using the Raineri–Friedman theory is excellent and gives confidence that the essential features of polar solvation are well understood.

We finally return to the much more complex case of the light harvesting complex LH2 shown in figure 1. In this system, which contains 27 BChl molecules in two rings of *ca.* 50Å diameter, one ring with nine (B800) and one ring with 18 (B850) BChls (McDermott *et al.* 1995; Jonas *et al.* 1995*a*), the model of dilute non-interacting chromophores is clearly inappropriate. Energy transfer occurs on multiple timescales in this complex from *ca.* 90 fs within the B850 ring to 700 fs for B800–B850 transfer (Jimanez *et al.* 1996). Transfer within the B800 ring occurs on a similar timescale (*ca.* 1 ps) (Monshouwer *et al.* 1995). The degree to which the electronic states of the B850 ring are delocalized around the ring has been extensively discussed (Chachisvilis *et al.* 1997; Kennis *et al.* 1996; Pullerits *et al.* 1996; Sauer *et al.* 1996; Bradforth *et*

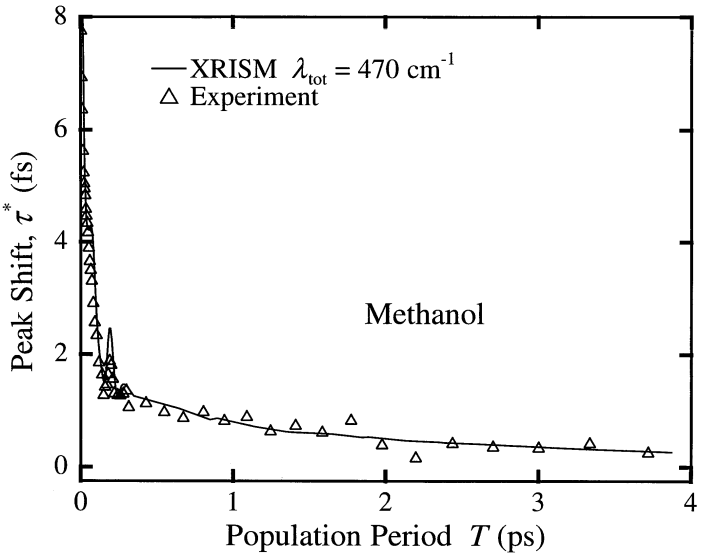


Figure 12. The three pulse echo peak shift of IR144 in methanol calculated using the $S(t)$ obtained via XRISM by Raineri & Friedman. The vibrational quantum beats obtained from fits of transient grating data (Joo *et al.* 1996*b*; Passino *et al.* 1997) are added to the theoretical curve to generate the full signal. The open triangles represent the data.

*al.* 1995; Novoderezhkin & Razjivin 1995; Visser *et al.* 1995). We have carried out 3PEPS studies on LH2 (B850) (Jimenez *et al.* 1997) and B800 (Joo *et al.* 1996*a*) as well as on the related LH1 (Jimenez *et al.* 1997) which contains a ring of 32 BChls absorbing at 875 nm (B875). The structure of the B875 ring is known only at low resolution (Karrasch *et al.* 1995), but is believed to be very similar to the B850 ring of LH2. It is possible to obtain subunits of LH1 containing two BChls which absorb at 820 nm (B820). This latter sample allows us to test for the role of energy transfer in determining the form of the peak shift signals.

No fully satisfactory theory exists as yet to describe 3PEPS signals on systems such as LH2, although Mukamel and co-workers are making rapid progress in this area (Meier *et al.* 1997). Our strategy in analysing the LH1 and LH2 data is to assume that energy transfer is manifest in the signals via its ability to disable rephasing that would otherwise occur in the inhomogeneous distribution of BChl rate energies. In other words, the energy transfer allows the excitation to visit sites that would have been inaccessible in its absence and effectively 'averages' over the inhomogeneous distribution. Thus, instead of the peak shift becoming constant after *ca.* 200 fs as it does for IR144 in PMMA (figure 5), the peak shift in LH1 and LH2 decays to zero. The energy transfer site can then be extracted from the $\tau^*$ versus $T$ data and gives *ca.* 90 fs from B875 and B850, in good agreement with fluorescence depolarization data (Jimenez *et al.* 1996; Bradforth *et al.* 1995). Details of this approach can be found in Jimenez *et al.* (1977). Recently, we have carried out 3PEPS experiments on the B820 subunit of LH1. Details of this experiment will be given elsewhere (Yu *et al.* 1997), and we briefly summarize it here. In striking contrast to LH1 and LH2, B820 where energy transfer cannot occur, gives a large long-time peak shift ($\tau^*(T \rightarrow \infty)$) consistent with significant inhomogeneous broadening (diagonal disorder). If the exponential component ascribed to energy transfer in the LH1 data simply has its time constant set to infinity, the fit parameters for LH1 describe B820

almost perfectly. In other words, the energy transfer component has now become inhomogeneous broadening and the consistency of the earlier analysis (Jimenez *et al.* 1997) is established.

## 3. Concluding remarks

The three pulse echo peak-shift technique has emerged as a sensitive and versatile probe of the interactions of chromophores with their environments whether they be liquids (de Boeij *et al.* 1995, 1996; Joo *et al.* 1996*a*,*b*; Passino *et al.* 1996), glasses (Nagasawa *et al.* 1997; Cho *et al.* 1996; Nagasawa *et al.* 1996) or proteins (Yu *et al.* 1997). In this article we have focused on polar liquid systems and illustrated the future of the harmonic bath model to describe the temperature dependence of the low-frequency portion of the spectral density. In contrast, the librational region of the spectral density (20–150 $\mathrm{cm}^{-1}$ in $\omega^2\rho(\omega)$) seems quite harmonic, both on lowering the temperature to 30 K in PMMA (Nagasawa *et al.* 1997) or raising it to 400 K in ethylene glycol (Passino *et al.* 1997). Molecular models of liquid dynamics, in particular the dynamical XRISM theory of Raineri & Friedman (Raineri *et al.* 1994, 1997; Friedman *et al.* 1994, 1995; Raineri & Friedman 1998), are intrinsically anharmonic in nature. The success of this model in reproducing 300 K data in both methanol and acetonitrile for both librational and diffusive regimes suggests that with appropriate input data from either simulation or dielectric dispersion and far infrared spectroscopy, the XRISM approach will be quantitative in predicting the dynamics of polar solvation.

This work was supported by a grant from NSF and in part by donors to the ACS Petroleum Research Fund. Y.N. was partly supported by JSPS during the course of this work and S.A.P. was a GAANN fellow. We thank Professor Minhaeng Cho (Korea University) for access to his unpublished results and comments on the manuscript and Harold Friedman and Fernando Raineri for providing us with their calculated solvation responses and for several important discussions.

## References

Bertie, J. E., Zhang, S. L., Eysel, H. H., Baluja, S. & Ahmed, M. K. 1993 *Appl. Spectroscopy* **47**, 1100.

Böttcher, C. J. F. & Bordewijk, P. 1978 *Theory of electric polarization*, vol. II. New York: Elsevier.

Bradforth, S. E., Jimenez, R., van Mourik, F., van Grondelle, R. & Fleming, G. R. 1995 *J. Phys. Chem.* **99**, 16 179.

Chachisvilis, M., Pullerits, T., Kühn, O. & Sundström, V. 1997 *J. Phys. Chem.* **101**, 7275.

Chandler, D. & Anderson, H. C. 1972 *J. Chem. Phys.* **57**, 1930.

Cho, M. & Fleming, G. R. 1998 *Adv. Chem. Phys.* (In the press.)

Cho, M., Fleming, G. R., Saito, S., Ohmine, I. & Stratt, R. M. 1994 *J. Chem. Phys.* **100**, 6672.

Cho, M., Yu, J.-Y., Nagasawa, Y., Passino, S. A. & Fleming, G. R. 1996 *J. Phys. Chem.* **100**, 11944.

de Boeij, W. P., Pshenichnikov, M. S. & Wiersma, D. A. 1995 *Chem. Phys. Lett.* **238**, 1.

de Boeij, W. P., Pshenichnikov, M. S. & Wiersma, D. A. 1996 *Chem. Phys. Lett.* **253**, 53.

Fleming, G. R. & Cho, M. 1996 *Ann. Rev. Phys. Chem.* **47**, 109.

Friedman, H. L., Perng, B.-C., Resat, H. & Raineri, F. O. 1994 *Phys. Cond. Matt.* A **6**, 131.

Friedman, H. L., Raineri, F. O., Hirata, F. & Perng, B.-C. 1995 *J. Stat. Phys.* **78**, 239.

Fröhlich, H. 1958 *Theory of dielectrics*. Oxford: Clarendon.

Gruebele, M. & Zewail, A. H. 1993 *J. Chem. Phys.* **98**, 883.

Horng, M. L., Gardecki, J. A., Papazayan, A. & Maroncelli, M. 1995 *J. Phys. Chem.* **99**, 17 311.

Jimenez, R., Dikshit, S. N., Bradforth, S. E. & Fleming, G. R. 1996 *J. Phys. Chem.* **100**, 6825.

Jimenez, R., van Mourik, F. & Fleming, G. R. 1997 *J. Phys. Chem.* B **101**, 7350.

Jonas, D. M. & Fleming, G. R. 1995 In *Ultrafast processes in chemistry and photobiology. Chem. 21 Century IUPAC* (ed. M. El-Sayed, I. Tanaka & Y. Molin), p. 225. Oxford: Blackwell.

Jonas, D. M., Bradforth, S. E., Passino, S. A. & Fleming, G. R. 1993 In *Proc. Royal Netherlands Academy Colloq. on Femtosecond Reaction Dynamics* (ed. D. A. Wiersma), p. 133. New York: Elsevier.

Jonas, D. M., Bradforth, S. E., Passino, S. A. & Fleming, G. R. 1995 *J. Phys. Chem.* **99**, 2594.

Joo, T., Jia, J., Yu, J.-Y., Jonas, D. M. & Fleming, G. R. 1996*a* *J. Phys. Chem.* **100**, 2399.

Joo, T., Jia, Y., Yu, J.-Y., Lang, M. L. & Fleming, G. R. 1996*b* *J. Chem. Phys.* **104**, 6089.

Jordan, B. P., Sheppard, R. J. & Szwarnowski, S. 1978 *J. Appl. Phys.* D **11**, 695.

Karrasch, S., Bullough, P. A. & Ghosh, R. 1995 *EMBO J.* **14**, 631.

Kennis, J. T. M., Strelsov, A. M., Aatsma, T. J., Nozawa, T. & Amesz, J. 1996 *J. Phys. Chem.* **100**, 2438.

Keyes, T. 1994 *J. Chem. Phys.* **101**, 5081.

Ladanyi, B. M. & Stratt, R. M. 1995 *J. Phys. Chem.* **99**, 2502.

Ladanyi, B. M. & Stratt, R. M. 1996 *J. Phys. Chem.* **100**, 1266.

Maeda, M. 1984 *Laser dyes*. New York: Academic.

Marcus, R. A. & Sutin, N. 1985 *Biochim. Biophys. Acta* **811**, 265.

McDermott, G., Prince, S. M., Freer, A. A., Hawthornthwaite-Lawless, A. M., Papiz, M. Z., Cogdell, R. J. & Isaacs, N. W. 1995 *Nature* **374**, 517.

Meier, T., Chrnyak, V. & Mukamel, S. 1997 *J. Chem. Phys.* **107**, 8759.

Monshouwer, R., Ortiz de Zarate, I., van Mourik, F. & van Grondelle, R. 1995 *Chem. Phys. Lett.* **246**, 341.

Mukamel, S. 1995 *Principles of nonlinear optical spectroscopy*. Oxford University Press.

Nagasawa, Y., Passino, S. A., Joo, T. & Fleming, G. R. 1996 *Ultrafast phenomena*. Berlin: Springer.

Nagasawa, Y., Passino, S. A., Joo, T. & Fleming, G. R. 1997 *J. Chem. Phys.* **106**, 4840.

Novoderezhkin, V. I. & Razjivin, A. P. 1995 *Biophys. J.* **68**, 1089.

Passino, S. A., Nagasawa, Y., Joo, T. & Fleming, G. R. 1996 *J. Phys. Chem.* **101**, 725.

Passino, S. A., Nagasawa, Y. & Fleming, G. R. 1997 *J. Chem. Phys.* **107**, 6094.

Pollard, W. T., Lee, S.-Y. & Mathies, R. A. 1990 *J. Chem. Phys.* **92**, 4012.

Pullerits, T., Chachisvilis, M. & Sundström, V. 1996 *J. Phys. Chem.* **100**, 10 787.

Raineri, F. O. & Friedman, H. L. 1998 *Adv. Chem. Phys.* (In the press.)

Raineri, F. O., Resat, H., Perng, B.-C., Hirata, F. & Friedman, H. L. 1994 *J. Chem. Phys.* **100**, 1477.

Raineri, F. O., Perng, B.-C. & Friedman, H. L. 1997 *Electrochimica Acta* **42**, 2749.

Rips, I., Klafter, J. & Jortner, J. 1988 *J. Chem. Phys.* **89**, 4288.

Sauer, K., Cogdell, R. J., Prince, S. M., Freer, A., Isaacs, N. W. & Scheer, H. 1996 *Photochem. Photobiol.* **64**, 564.

Scherer, N. F., Jonas, D. M. & Fleming, G. R. 1993 *J. Chem. Phys.* **99**, 153.

Stratt, R. M. 1995 *Acc. Chem. Res.* **28**, 201.

Stratt, R. M. & Cho, M. 1994 *J. Chem. Phys.* **100**, 6700.

Visser, H. M., Somsen, O. J. G., van Mourik, F., van Stokkum, I. H. M. & van Grondelle, R. 1995 *Biophys. J.* **69**, 1083.

Wolynes, P. G. 1987 *J. Chem. Phys.* **86**, 5133.

Yu, J.-Y., Nagasawa, Y., van Grondelle, R. & Fleming, G. R. 1997 *Chem. Phys. Lett.* **280**, 404.